Fluorination and reduction of CaCrO3 by topochemical methods

Journal:	*Dalton Transactions*
Manuscript ID	DT-ART-11-2019-004321.R1
Article Type:	Paper
Date Submitted by the Author:	17-Jan-2020

Complete List of Authors:	Juillerat, Christian; University of South Carolina, Department of Chemistry and Biochemistry Tsujimoto, Yoshihiro; National Institute fo Materials Science, Research Center for Functional Materials; Hokkaido University, Graduate School of Chemical Sciences and Engineering Chikamatsu, Akira; The University of Tokyo, Department of Chemistry Masubuchi, Yuji; Hokkaido University, Graduate School of Engineering Hasegawa, Tetsuya; Graduate School of Engineering, Department of Material and Life Science Yamaura, Kazunari; National Institute for Materials Science, ; Hokkaido University,

Fluorination and reduction of $CaCrO_3$ by topochemical methods

Christian A. Juillerat,[1, 2*] Yoshihiro Tsujimoto,[1, 3*] Akira Chikamatsu,[4] Yuji Masubuchi,[5] Tetsuya Hasegawa,[4] Kazunari Yamaura[1, 3]

[1] *Research Center for Functional Materials, National Institute for Materials Science, 1-1 Namiki, Tsukuba, Ibaraki 305-0044, Japan*
[2] *Department of Chemistry and Biochemistry, University of South Carolina, Columbia, South Carolina 29208, USA*
[3] *Graduate School of Chemical Sciences and Engineering, Hokkaido University, North 13 West 8, Kita-ku, Sapporo 060-0808, Japan*
[4] *Department of Chemistry, The University of Tokyo, 7-3-1 Hongo, Bunkyo-ku, Tokyo 113-0033, Japan*
[5] *Faculty of Engineering, Hokkaido University, North 13 West 8, Kita-ku, Sapporo 060-8628, Japan*

*Corresponding authors
Email: juillerc@email.sc.edu, TSUJIMOTO.Yoshihiro@nims.go.jp

Abstract: Topochemical reactions between $CaCrO_3$ and polyvinylidene difluoride yield the new fluorinated phase $CaCrO_{2.5}F_{0.5}$, which was characterized by powder synchrotron X-ray diffraction, X-ray photoemission spectroscopy, and magnetic susceptibility measurements. The reaction proceeds via reduced oxide intermediates, $CaCrO_{2.67}$ and $CaCrO_{2.5}$, in which CrO_6 octahedral and CrO_4 tetrahedral layers are stacked in a different manner along the *c* axis of $CaCrO_3$. These two intermediate phases can be selectively synthesized by the carbothermal reduction with g-C_3N_4. Both $CaCrO_3$ and $CaCrO_{2.5}F_{0.5}$ adopt the same orthorhombic space group, *Pbnm*; however, the fluorinated phase has decreased Cr-O-Cr bond angles as compared to the parent compound in both the *ab* plane and along the *c*-direction, which indicates an increased orthorhombic distortion due to the fluorination. While the oxygen vacancies are ordered in both intermediate phases, $CaCrO_{2.67}$ and $CaCrO_{2.5}$, a site preference for fluorine in the oxyfluoride phase cannot be confirmed. $CaCrO_3$ and $CaCrO_{2.5}F_{0.5}$ undergo antiferromagnetic phase transitions involving spin canting, where the fluorination causes the transition temperature to increase from 90 K to 110 K, as a result of the competition between the increased octahedral tilting and the enhancement of superexchange interactions involving Cr^{3+} ions in the $CaCrO_{2.5}F_{0.5}$ structure.

Introduction:

Recently, the development of topochemical techniques have allowed for the facile synthesis of phases with new anion lattices or metal coordination geometries in oxides, the synthesis of which has been central in solid state chemistry, as it expands our knowledge of structure property relationships.[1] A number of oxygen deficient or oxyfluoride phases have been obtained by treating oxides normally obtained easily by solid state reactions with either a reducing or fluorinating agent.[2, 3] Topochemical reduction using an alkali/alkaline hydride yields novel oxyhydrides and oxygen-vacancy ordered compounds. For example, $LaSr_3NiRuO_4H_4$ with metal hydride sheets and AFeO$_2$ (A = Ca, Sr, Ba) with square-planar oxides [4] are obtained from the corresponding oxide phases.[5–7] Low-temperature fluorination reactions using fluorine gas, fluoropolymer or a binary metal fluoride also allow for unique anion-lattice modification via the substitution of fluorine for oxygen and/or fluorine insertion,[8] as exemplified by the synthesis of superconducting $Sr_2CuO_2F_{2+\delta}$ from Sr_2CuO_3. [9]

Applying these topochemical methods to materials obtained from high-pressure synthesis, a 'hard-soft' synthetic approach, is under explored and can lead to the exploration of metal coordination environments that aren't readily accessible at ambient pressures. For example, it is well known the tetravalent chromium cation strongly favors tetrahedral coordination over octahedral coordination and the ionic radius is too small to be incorporated into perovskite structures, although these observations are not without exceptions.[10] Previously, alkaline chromium oxide perovskites such as ACrO$_3$ (A = Ca, Sr) have been stabilized under high pressures,[11, 12] and Arevalo-Lopez and Attfield *et al.* have discovered new oxygen-vacancy ordered phases $CaCrO_{3-x}$ (x = 0.33, 0.4, 0.5)[13, 14] and $SrCrO_{3-y}$ (y = 0.2, 0.25), [15] which were synthesized by reduction of $ACrO_3$ (A = Ca, Sr) with hydrogen gas. $CaCrO_{2.5}$ was found to adopt the brownmillerite structure. These oxygen deficient layers depend on the A site cations: vacancies in $CaCrO_{3-x}$ are formed in the (001) plane of the cubic perovskite structure, but vacancies in $SrCrO_{3-y}$ are formed in the (111) plane (Figure 1).

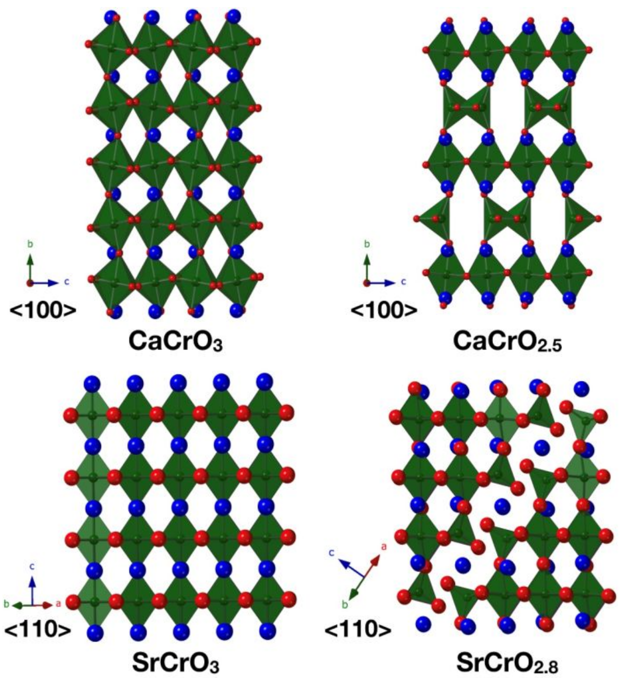

Figure 1. Structures of $ACrO_3$ (A = Ca, Sr) and their reduced products obtained by reductive reactions carried out with g-C_3N_4. $CaCrO_{2.5}$ adopts the brownmillerite structure. Chromium octahedra are shown in green, oxygen atoms in red, and A atoms in blue.

Very recently, our research group reported the topochemical fluorination of $SrCrO_3$ with polyvinylidene difluoride (PVDF), which involved the formation of $SrCrO_{2.8}$ as an intermediate oxide.[16] The layers of tetrahedrally coordinated Cr^{4+} in $SrCrO_{2.8}$ create a pathway for the subsequent fluorine insertion, and the resulting oxyfluoride phase was the cubic $SrCrO_{2.8}F_{0.2}$ with fluoride ions randomly distributed in the structure. Furthermore, $SrCrO_{2.8}$ could be isolated for the first time by topochemical reduction with g-C_3N_4.[16] It should be noted that the degree of fluorination in $SrCrO_3$ seems to be restricted by the amount of the oxygen deficiencies in the intermediate phase. Thus, to gain deeper understanding of the fluorination mechanism for $SrCrO_3$, it is useful to perform chemical substitution in the parent materials and explore the different types of oxygen deficient phases obtained by reduction.

In this study, we report the fluorination and reduction of $CaCrO_3$ with PVDF and g-C_3N_4, which revealed stepwise fluorination processes similar to that for $SrCrO_3$ but different pathways for oxygen removal and fluorine insertion as well as higher degree of fluorination.

Experimental

Synthesis. $CaCrO_3$ powder was obtained using a multi-anvil high-pressure method previously reported by Weiher *et al.*[11] $CaCO_3$ was heated over night at 1000 °C in air to obtain CaO, which was combined stoichiometrically with CrO_2 (Aldrich) in an Ar filled glovebox and loaded into a Pt capsule. The Pt capsule was loaded into a high-pressure cell and heated at 900 °C under a pressure of 5 GPa for 1 h before quenching to room temperature by turning off the heat before releasing the pressure. The black polycrystalline product, $CaCrO_3$, contained a $CaCr_2O_4$ impurity (13 wt.%) and was fluorinated using PVDF (Aldrich) in molar ratios of 0.1 to 0.5 (PVDF/$CaCrO_3$). PVDF and $CaCrO_3$ were mixed, pelletized, and sealed in a glass tube under vacuum before heating at temperatures of 350, 370, and 400 °C. $CaCrO_3$ was also reduced using g-C_3N_4 (synthesized in house) in ratios of 0.25 (C_3N_4/$CaCrO_3$) following a similar procedure.

Structure. The structures of the resulting powders were analyzed by Rietveld refinement using synchrotron X-ray powder diffraction (SXRD) data collected at room temperature using one-dimensional X-ray detectors installed on BL15XU, NIMS beamline at SPring-8 in Japan. The synchrotron radiation X-rays were monochromatized to the wavelength of 0.65298 Å. The samples were loaded in glass capillaries and inner diameter of 0.1mm, and the diffraction data were recorded in 0.003° increments over the range of $4 \leq 2\theta \leq 60°$. Structure refinements were performed using the Rietveld method with the program RIETAN-FP.[17] X-ray Photoemission spectroscopy (XPS) measurements were performed by using Mg $K\alpha$ X-ray source (JEOL JPS-9010MC). The Fermi level was calibrated using the C1s signal.

Results and Discussion

Synthesis. For both post-synthetic fluorination and reductive reactions, a temperature of 400 °C produced better results, although the reactions can be carried out at 350 and 370 °C but the reactions did not reach completion at these temperatures. The reactions of $CaCrO_3$ with PVDF at different ratios show a stepwise fluorination of $CaCrO_3$, where $CaCrO_3$ is first reduced to $CaCrO_{2.67}$ and $CaCrO_{2.5}$, before the fluorinated phase forms (see Figure 2). At ratios of 0.1 and 0.2 (PVDF/$CaCrO_3$) $CaCrO_{2.67}$ and $CaCrO_{2.5}$ are formed, and these phases disappear as the fluorinated phase, $CaCrO_{3-x}F_x$, begins to form at a ratio of 0.3 (PVDF/$CaCrO_3$). These behaviors suggest that fluorine is inserted into the tetrahedral layers of $CaCrO_{2.5}$. The fluorinated phase obtained at 0.5 (PVDF/$CaCrO_3$) can be assigned to an orthorhombic cell with a = 5.34098(9) Å, b = 5.40324(9) Å, and c = 7.53180(10) Å. Low-temperature reduction using g-C_3N_4 was also examined on $CaCrO_3$, which resulted in the successful isolation of $CaCrO_{2.5}$ and $CaCrO_{2.67}$ under controlled reaction temperatures, although a few uncharacterized peaks, which disappear at higher temperatures, were detected in $CaCrO_{2.67}$ as indicated in the right panel of Fig. 2. We notice that both the fluorination and reduction of $CaCrO_3$ causes peak broadening, which is probably due to a reduced crystallinity through the topochemical reactions.

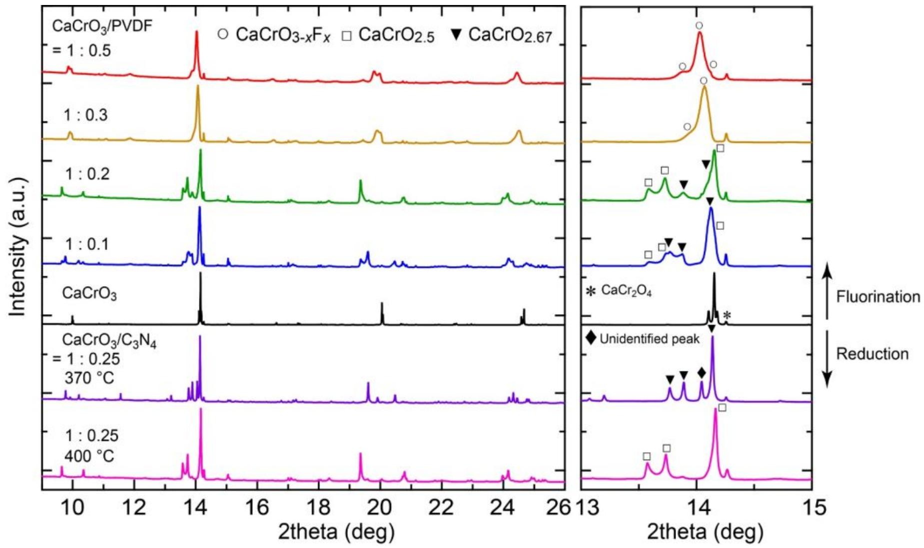

Figure 2. SXRD patterns of the products obtained by reactions of $CaCrO_3$ with PVDF or g-C_3N_4. $CaCrO_3$ is fluorinated via two oxygen deficient phases, i.e. $CaCrO_{2.67}$ and $CaCrO_{2.5}$. These reduced phases can be isolated by controlling the reaction temperature with g-C_3N_4.

Structure. Figure 3 shows the result of Rietveld refinement against the PXRD data collected from the product obtained by the reaction of $CaCrO_3$ with PVDF at 400 °C. Even after the fluorination reaction, the structure retained the orthorhombic space group *Pbnm*, but the lattice constants increased by 0.98, 1.60, and 0.60% along *a*, *b*, and *c* directions, respectively. The variation in volume ($\Delta V/V$) is 3.2%, which is larger than the volume change between $SrCrO_3$ and $SrCrO_{2.8}F_{0.2}$ (2.5%) but smaller than that between $SrFeO_3$ and $SrFeO_2F$ (8.2%).[15, 16] No additional peaks associated with O/F anion ordering were detected. For structural refinement of the oxyfluoride phase, the crystal structure of $CaCrO_3$ was used as a starting model. No attempt was made to distinguish oxide and fluoride ions because of their similar X-ray scattering factors. $CaCr_2O_4$ and CaF_2 were also added to the refinement as secondary phases. The refinement readily converged well to R_{wp} = 2.01% and R_B = 3.73 %. No anion-site deficiencies were found within the error margin, indicating that the oxygen vacant sites in $CaCrO_{2.5}$ were completely filled with fluoride ions. Thus, the expected chemical composition is $CaCrO_{2.5}F_{0.5}$, implying higher degree of fluorination than that for $SrCrO_3$.[16] Rietveld refinements were performed on PXRD data collected on the parent structure, $CaCrO_3$, and the reduced structure, $CaCrO_{2.5}$, and are shown in Figures S1 and S2, although there are no new results considering both structures have previously been thoroughly characterized.[14,11,18] The refined atomic coordinates for $CaCrO_{2.5}F_{0.5}$, $CaCrO_3$, and $CaCrO_{2.5}$ are shown in Tables S1-3.

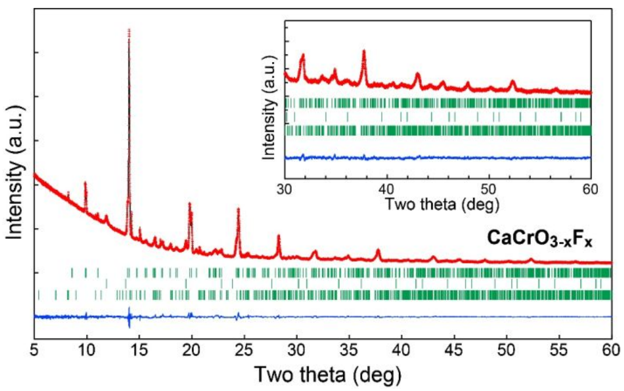

Figure 3. Rietveld refinement against the PXRD data collected from the fluorinated product at room temperature. The observed (red crosses), calculated (black solid line), and difference (blue solid line) plots are shown. The vertical lines represent the fluorinated phase (81%), CaF_2 (12%), and $CaCr_2O_4$ (7%) from top to bottom. The inset shows an enlarged plot in a high 2θ region.

We investigated the change in oxidation state of the chromium ions due to the fluorination of $CaCrO_3$ by XPS measurements. Figure 4 shows the Cr 2*p* spectra collected from $CaCrO_3$ and its fluorinated phase. The Cr $2p^{3/2}$ spectrum of $CaCrO_3$ is decomposed into three components which could be assigned as Cr^{3+}, Cr^{4+}, and Cr^{6+} with binding energies of 576.38, 578.96, and 582.35 eV, respectively.[19] The trivalent and tetravalent chromium should be derived from $CaCr_2O_4$ and $CaCrO_3$, respectively. The atomic ratio of Cr^{3+} to Cr^{4+} estimated from the spectral area is 0.15:0.80, which agrees well with that obtained from the Rietveld analysis (0.17:0.83). The Cr^{6+} species, which were not detected by the SXRD pattern, should be attributed to surface defects. For the oxyfluoride phase, the Cr $2p^{3/2}$ spectrum can be decomposed into Cr^{3+} and Cr^{4+} species in an atomic ratio of 0.40:0.60. The increase in the Cr^{3+} component is consistent with O-to-F substitution in $CaCrO_3$. However, the atomic ratio of Cr^{3+} to Cr^{4+} determined by XPS (0.40:0.60) deviates from that estimated from the PXRD analysis (0.50:0.50) assuming the oxyfluoride phase as $CaCrO_{2.5}F_{0.5}$. This discrepancy is likely due to the low signal-to-noise ratio caused by residual C-F species from the fluorinating agent, as seen from the wide-scan spectra in Figure S3.

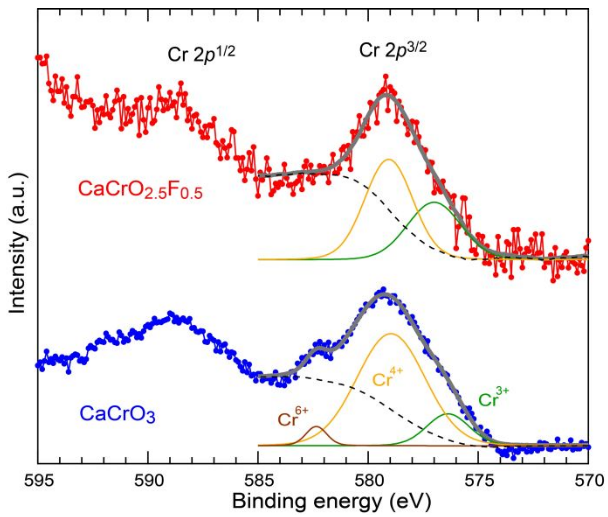

Figure 4. Cr 2*p* core level photoelectron spectra collected from $CaCrO_3$ and its fluorinated phase at 300 K. The bold grey and dashed black lines represent the fitting curves and the Shirley background, respectively. The green, orange, and brown solid lines correspond to Cr^{3+}, Cr^{4+} and Cr^{6+} components.

The structure of $CaCrO_3$ is well studied and adopts the ABO_3 perovskite structure with an orthorhombic distortion due to the small size of the Ca^{2+} ion,[18, 20] as compared to the cubic $SrCrO_3$, and crystallizes in the *Pbnm* space group with lattice parameters a = 5.28912(1) Å, b = 5.31796(1) Å, and c = 7.48677(1) Å. The oxygen vacancies are ordered in $CaCrO_{2.5}$ and $CaCrO_{2.67}$, creating layers of Cr octahedra and tetrahedra (Figure 5). In $CaCrO_{2.67}$, the tetrahedral layer occurs every third layer, while in $CaCrO_{2.5}$, which adopts the brownmillerite structure, it occurs every other layer. The relationship of the octahedral layers to the tetrahedral layers can be understood as the removal of every other infinite chain of oxygen atoms as illustrated in Figure 5. This reduces the coordination of Cr from 6 to 4, and as a result the Cr-O-Cr bond which is nearly linear in the octahedral layers contracts to form the approximately 109° bond angle found in tetrahedral coordination environments.

Rietveld refinement against the SXRD data of $CaCrO_{2.5}F_{0.5}$ revealed all of the anion sites in the ABO_3 structure were fully occupied upon fluorination and $CaCrO_{2.5}F_{0.5}$ adopted the same space group of the parent compound. The structure symmetry allows anions to occupy two unique sites, namely the sites on the *ab* plane ($X1$) and along the *c* axis ($X2$). Thus, the existence of a selective fluorine distribution over the anion sites cannot be ruled out. To examine the possible anion ordering of O/F ions, bond-valence-sum (BVS) calculations were carried out on the assumption of three types of fluorine distribution, namely, on $X1$, $X2$, or both sites. The BVS values for all atoms are summarized in Table S4. Unfortunately, we could not conclude any types of anion ordering: the BVS values for $X1$ and $X2$ sites as well as Ca and Cr sites were consistent with the assumed fluorine distribution patterns.

Figure 6 shows a comparison between the refined crystal structures of $CaCrO_3$ and $CaCrO_{2.5}F_{0.5}$. Hereafter, the full anion disordered model is employed to discuss the structure and properties of the oxyfluoride phase, since no selective fluorine distribution was observed. All the Cr-F/O bond lengths are increased from 1.9002(4), 1.911(1), and 1.912(1) Å to 1.935(1), 1.960(4), and 1.919(4) Å (see Figure 6). These behaviors are consistent with the increased Cr^{3+}/Cr^{4+} via the substitution of fluorine for oxygen. The oxyfluoride structure also contains tightened Cr-O/F-Cr bond angles of 156.6(2) and 153.3(3)° as compared to 157.70(8) and 160.13(13)° in the parent structure. A higher degree of the octahedral tilting in the fluorinated perovskite can be accounted for by considering Goldschmidt's tolerance factor (t), which is expressed as $t = (r_A+r_X)/\sqrt{2}(r_B+r_X)$.[21, 22] The r_A, r_B, and r_X are the Shannon's ionic radii of A-site cation, B-site cation, and X-site anion.[22] The calculated t factor of $CaCrO_{2.5}F_{0.5}$ is 0.979, lower than more ideal value of $CaCrO_3$ ($t = 0.994$).

Although no examples of *B*-O-*B* bond angle compression upon fluorinating could be found for chromium oxides, $LaSrCoFeO_5F$ contains tightened (Co/Fe)-(O/F)-(Co/Fe) bond angles as compared to the oxygen-stoichiometric oxide $LaSrCoFeO_6$, both of which adopt the trigonal space group *R*-3*c*. [23] $La_{0.5}Sr_{0.5}FeO_{2.5}F_{0.5}$, which crystalizes in the lower symmetry *Pnma* as compared to the oxide which adopts the *R*-3*c* space group, also exhibits similar changes in local coordination around the metal center where the Fe-O-Fe bond angles contract from 167.0(3) to 163. 39(11) and 159.68(13) and the Fe-O bond distances increase from 1.9567(6) to 1.996(4), 1.9996(6), and 1.986(4), upon fluorination. [24]

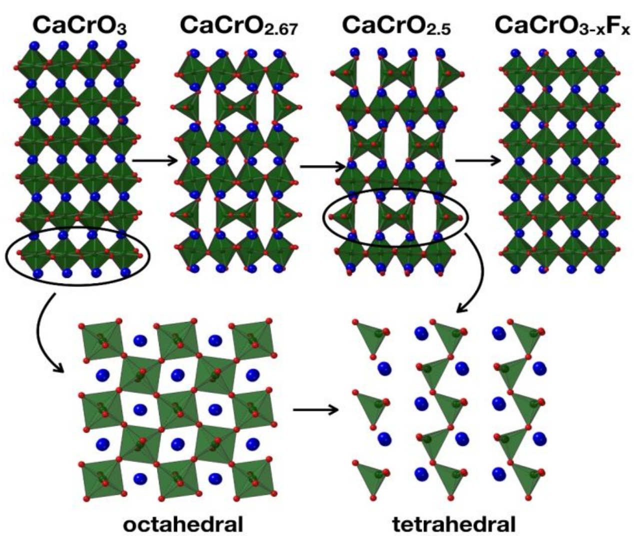

Figure 5. Structures of $CaCrO_3$, $CaCrO_{2.5}$, $CaCrO_{2.67}$, and $CaCrO_{3-x}F_x$ showing the sequences of octahedral and tetrahedral layers as a result of oxygen vacancies where chromium octahedra are shown in green, oxygen atoms in red, and calcium atoms in blue.

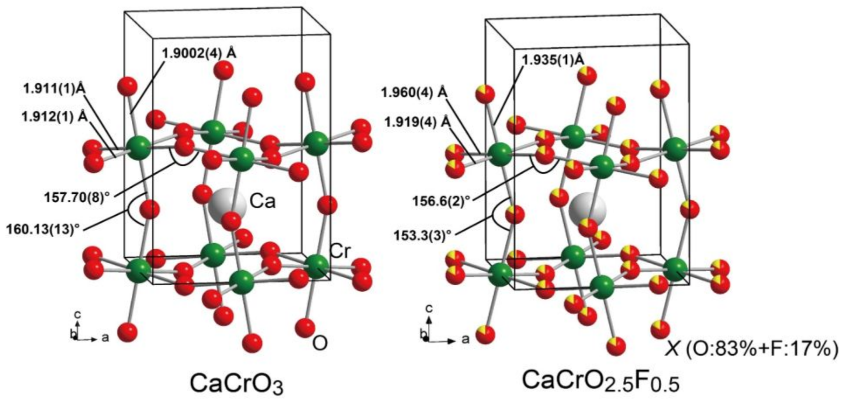

Figure 6: Detailed view of chromium coordination environments in $CaCrO_3$ and $CaCrO_{3-x}F_x$ where the Cr atoms are shown in green, oxygen atoms in red, and the calcium atoms in white.

Reaction pathway. $CaCrO_3$ exhibited stepwise fluorination processes as observed in $SrCrO_3$.[16] However, the important differences between the fluorination mechanisms of $CaCrO_3$ and $SrCrO_3$ are as follows, (1) the degree of fluorination for $CaCrO_3$ is higher than that for $SrCrO_3$, (2) the formation of two intermediate oxide phases of x = 0.33 and 0.5 are involved, and (3) the plane where oxygen removal and fluorine insertion occurs is (001) for $CaCrO_3$ but (111) for $SrCrO_3$. It is apparent that the larger amount of fluorine atoms inserted into $CaCrO_3$ is attributable not only to its deoxidation capacity but also the reducing power of PVDF. Indeed, the first reduced phase $CaCrO_{2.67}$ is subsequently reduced to $CaCrO_{2.5}$ prior to the fluorination, whereas for the fluorination of $SrCrO_3$ the first reduced phase $SrCrO_{2.8}$ is not further reduced to $SrCrO_{2.75}$ but directly fluorinated to $SrCrO_{2.8}F_{0.2}$. The pathway of the oxygen removal and fluorine insertion for $CaCrO_3$, which is different from those for $SrCrO_3$, also play an important role in the formation of the highly fluorinated phase $CaCrO_{2.5}F_{0.5}$. The fluorine insertion mechanism remains an open question. If fluorine atoms simply occupy the oxygen vacant sites, a partial O/F order on the X1 sites is realized. In contrast, fluorine insertion involving migration of apical oxygen, which was observed for layered perovskite compounds,[9, 25] would result in a partial anion order on the X2 sites or the full anion disorder. Mitra et al. investigated the oxygen diffusion pathways in brownmillerite $SrCoO_{2.5}$ by first-principle calculations, and found that the one-dimensional-ordered oxygen vacant channels in the CoO_4 tetrahedral layers provide the easiest diffusion pathway compared with the directions perpendicular to the vacant channels.[25] Based on this study, it is likely that fluorine also migrates and resides in the CrO_4 tetrahedral layers. Similar to the observed O/F disorder in $SrCrO_{2.8}F_{0.2}$, the oxygen-deficiency ordered structures do not influence the fluorine sites, perhaps due to the transformation of the Cr coordination from tetrahedron to octahedron which causes the rearrangement of the fluorine atom positions. Similar fluorine migration during fluorination reaction is observed in related perovskite compounds.[9, 26, 27]

Magnetism. Figure 7 shows the temperature dependence of the magnetic susceptibility χ (= M/H) of $CaCrO_3$, $CaCrO_{2.5}$, and $CaCrO_{2.5}F_{0.5}$, measured under zero-field-cooled (ZFC) and field-cooled (FC) conditions in the temperature range between 5 and 300 K. Anomalies in the magnetic susceptibility of the samples, or the inverse, from the magnetic impurity, $CaCr_2O_4$, with features at 100 K and 21 K,[28] were not observed indicating that $CaCr_2O_4$ did not significantly impact the susceptibility data. The χ (T) of $CaCrO_3$ exhibited a sudden increase at T_N = 90 K followed by a divergence between ZFC and FC data. These behaviors can be accounted for by a canted antiferromagnetism.[18] The weak temperature dependence above T_N, which does not obey the Curie-Weiss law, is consistent with the metallic state unambiguously characterized by spectroscopic techniques.[20, 29] For $CaCrO_{2.5}$, a small cusp associated with an antiferromagnetic ordering was observed at around 240 K in the ZFC data. The T_N value is close to that determined by the neutron diffraction analysis in Attfield *et al.*.[14] The small anomaly in the susceptibility at T_N is probably due to the decrease in crystallinity during the reductive reaction. In contrast to $CaCrO_{2.5}$, the χ (T) of $CaCrO_{2.5}F_{0.5}$ is similar to that of $CaCrO_3$: an antiferromagnetic phase transition involving spin canting was observed at 110 K. The moderate increase in χ (T) below T_N suggests decreased spin canting angles between Cr ions. It should be noted the high temperature data above T_N cannot be described again by the Curie-Weiss law, although it is somewhat more dependent on temperature than that of $CaCrO_3$. In fact, the Curie-Weiss fit gave the Curie constant C = 4.17(1) (emu K)/mol, which is unphysically large compared to the value expected from localized magnetic moments of Cr(III) with S = 3/2 and Cr(IV) with S = 1. This behavior suggests that the oxyfluoride has a metallic state like $CaCrO_3$ or insulating state located near the border between metallic and insulating phases. Unfortunately, even the cold-pressed sample after fluorination was so fragile that electrical measurements could not be performed. In light of the fact that $CaCrO_3$ resides near the crossover regime from itinerant to localized electron system,[18] the O-to-F substitution involving a decrease in the Cr-O-Cr tilt angles and lowered *pd* hybridization via more electronegative fluoride would shift the chromium perovskite to an insulating phase. Similar enhanced Pauli paramagnetic behaviors are observed in early 3*d*-transition metal insulators such as $LaTiO_3$ and $LaVO_3$, [30, 31] which are assumed to be near the metal-insulator transition.

The impact of fluorination on the magnetism greatly differs between $CaCrO_3$ and $SrCrO_3$.[16] In $SrCrO_3$ showing a Pauli paramagnetic behavior, replacement of 6.7% of oxygen sites with fluorine induces an antiferromagnetic ordered state with T_N = 230 K. In contrast, the fluorination of $CaCrO_3$ increased the magnetic ordering temperature by only 20 K despite the substitution of 16.7% oxygen for fluorine. The difference can be rationalized by considering variations in Cr–(O/F)–Cr bond angles and the oxidation number of Cr ions. In $SrCrO_{2.8}F_{0.2}$ with a cubic structure, the Cr–(O/F)–Cr bond angles are 180°, which maximizes the superexchange interactions between Cr ions. Moreover, the presence of Cr^{3+} ions via the fluorination insertion contributes to the enhancement of magnetic interactions. As a result, the high Néel ordering temperature is obtained. In

$CaCrO_{2.5}F_{0.5}$, however, Cr–(O/F)–Cr bond angles both along the *c* axis and on the *ab* plane become smaller via fluorination, which weakens the nearest neighbor interactions. Thus, the moderate increase in T_N observed in $CaCrO_{2.5}F_{0.5}$ should result from a competition between the increased octahedral tilting and the enhancement of superexchange interactions involving Cr^{3+} ions.

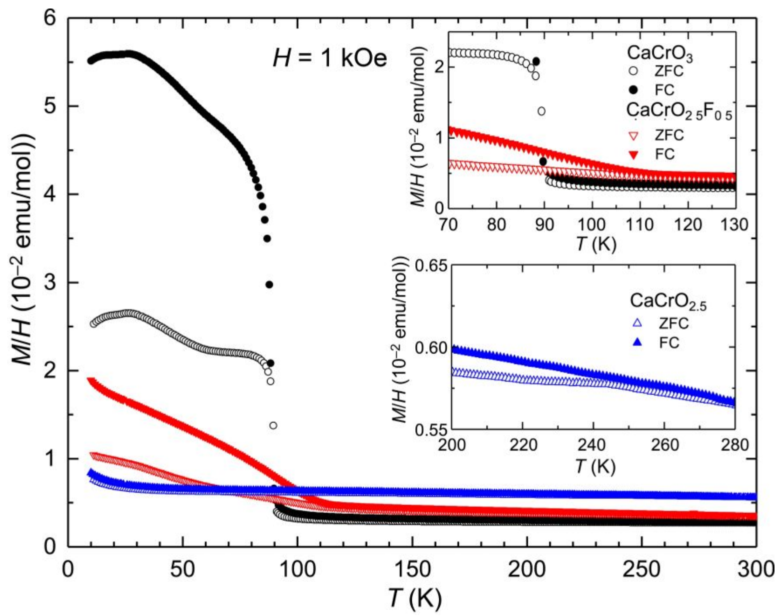

Figure 7. Temperature dependence of the magnetic susceptibility of $CaCrO_3$, $CaCrO_{2.5}$, and $CaCrO_{2.5}F_{0.5}$, measured under zero field cooled and field cooled conditions. The insets highlight anomalies associated with the magnetic phase transitions.

Conclusion

In this study, the new fluorinated phase, $CaCrO_{2.5}F_{0.5}$, was isolated by reacting $CaCrO_3$ with PVDF at 400 °C. This reaction proceeds via reduced oxide intermediate phases $CaCrO_{2.67}$ and $CaCrO_{2.5}$, which can be obtained by reacting $CaCrO_3$ with g-C_3N_4. The degree of fluorination for $CaCrO_3$ is higher than that for $SrCrO_3$, which is attributed to the deoxidation capacity that is more easily maximized by PVDF. The structure of $CaCrO_{2.5}F_{0.5}$ was characterized by synchrotron powder diffraction and adopts the same structure as $CaCrO_3$ with slightly larger lattice parameters with no detectable O/F ordering. This structure is supported by the XPS results which reveal Cr^{3+}/Cr^{4+} ratios close to the expected value of 0.5/0.5 for the proposed $CaCrO_{2.5}F_{0.5}$ structure based on full anion site occupancy. Magnetic measurements reveal that the fluorinated product has an increased spin-canted antimagnetic phase transition temperature as compared to $CaCrO_3$, which is due to the competition between the increased octahedral tilting and the enhancement of superexchange interactions involving Cr^{3+} ions in the $CaCrO_{2.5}F_{0.5}$ structure.

Supporting Information

The supporting in formation contains plots for the Rietveld refinements and tables atomic positions of $CaCrO_3$ and $CaCrO_{2.5}$, a wide scan XPS spectra for $CaCrO_3$ and $CaCrO_{2.5}F_{0.5}$, and inverse magnetic susceptibility plots for all three compounds.

Acknowledgements

This work was supported by the JSPS KAKENHI (Grant no. JP15H02024, JP16H06438, JP16H06441, JP19H02594, 19H04711, 16H06439, 16K21724), a research grant from Innovative Science and Technology Initiative for Security, ATLA, Japan. The SXRD experiments at SPring-8 were performed with the approval of JASRI (Proposal no. 2019A4501). C Juillerat was additionally supported by an NSF IGERT Graduate Fellowship under grant number 1250052 and by the U.S. Department of Energy, Office of Basic Energy Sciences, Division of Materials Sciences and Engineering under Award DE-SC0016574.

References

(1) Kageyama, H.; Hayashi, K.; Maeda, K.; Attfield, J. P., Expanding frontiers in materials chemistry and physics with multiple anions, *Nature Communications* **2018**, *9*, 772.

(2) Hayward, M. A., Synthesis and Magnetism of Extended Solids Containing Transition-Metal Cations in Square-Planar, MO_4 Coordination Sites, *Inorg. Chem.* **2019**, *58*, 11961-11970.

(3) Tsujimoto, Y.; Yamaura, K.; Takayama-Muromachi, E., Oxyfluoride chemistry of layered perovskite compounds, *Applied Sciences* **2012**, *2*, 206-219.

(4) Jin, L.; Lane, M.; Zeng, D.; Kirschner, F. K. K.; Lang, F.; Manuel, P.; Blundell, S.; McGrady, J.; Hayward, M. A., $LaSr_3NiRuO_4H_4$: A 4d Transition-Metal Oxide–Hydride Containing Metal Hydride Sheets, *Angew. Chem.* **2018**, *57*, 5025-5028.

(5) Tsujimoto, Y.; Tassel, C.; Hayashi, N.; Watanabe, T.; Kageyama, H.; Yoshimura, K.; Takano, M.; Ceretti, M.; Ritter, C.; Paulus, W., Infinite-layer iron oxide with a square-planar coordination, *Nature* **2007**, *450*, 1062-1065.

(6) Tassel, C.; Pruneda, J. M.; Hayashi, N.; Watanabe, T.; Kitada, A.; Tsujimoto, Y.; Kageyama, H.; Yoshimura, K.; Takano, M.; Nishi, M.; Ohoyama, K.; Mizumaki, M.; Kawamura, N.; Íñigues, J.; Canadell, E., $CaFeO_2$: A New Type of Layered Structure with Iron in a Distorted Square Planar Coordination, *J. Am. Chem. Soc.* **2008**, *131*, 221-229.

(7) Yamamoto, T.; Kobayashi, Y.; Hayashi, N.; T, S.; Yamanaka, S.; Takano, M.; Ohoyama, K.; Shimakawa, Y.; Yoshimura, K.; Kageyama, H., $(Sr_{1-x}Ba_x)FeO_2$ ($0.4 \leq x \leq 1$): A New Oxygen-Deficient Perovskite Structure, *J. Am. Chem. Soc.* **2012**, *134*, 11444-11454.

(8) Clemens, O.; Slater, P. R., Topochemical modifications of mixed metal oxide compounds by low-temperature fluorination routes, *Reviews in Inorganic Chemistry* **2013**, *33*, 105-117.

(9) Ai-Mamouri, M.; Edwards, P. P.; Greaves, C.; Slaski, M., Synthesis and superconducting properties of the strontium copper oxy-fluoride $Sr_2CuO_2F_{2+\delta}$, *Nature* **1994**, *369*, 382-384.

(10) Zhang, R.; Read, G.; Lang, F.; Lancaster…, T., $La_2SrCrO_7F_2$: A Ruddlesden–Popper Oxyfluoride Containing Octahedrally Coordinated Cr^{4+} Centers, *Inorg. Chem.* **2016**, *55*, 3169-3174.

(11) Weiher, J. F.; Chamberland, B. L.; Gillson, J. L., Magnetic and electrical transport properties of CaCrO3, *J. Solid State Chem.* **1971**, *3*, 529-532.

(12) Chamberland, B. L., Preparation and properties of $SrCrO_3$, *Solid State Commun.* **1967**, *5*, 663-666.

(13) Arevalo-Lopez, A. M.; Liang, B.; Senn, M. S.; Murray, C.; Tang, C.; Attfield, J. P., Hard–soft synthesis of a new series of vacancy-ordered perovskites, $CaCrO_{3-\partial}$, *J. Mater. Chem. C* **2014**, *2*, 9364-9367.

(14) Arevalo-Lopez, A. M.; Attfield, J. P., Crystal and magnetic structures of the brownmillerite $Ca_2Cr_2O_5$., *Dalton Trans.* **2015**, *44*, 10661-10664.

(15) Arévalo-López, A. M.; Rodgers, J. A.; Senn, M. S.; Sher, F.; Farnham, J.; Gibbs, W.; Attfield, J. P., "Hard-soft" synthesis of $SrCrO_{3-\delta}$ superstructure phases., *Angew Chem Int Ed Engl* **2012**, *51*, 10791-10794.

(16) Su, Y.; Tsujimoto, Y.; Fujii, K.; Masubuchi, Y.; Ohata, H.; Iwai, H.; Yashima, M.; Yamaura, K., Stepwise topochemical fluorination of $SrCrO_3$ perovskite a super-structured oxide, *Chem. Commun.* **2019**, *55*, 7239-7242.

(17) Izumi, F.; Momma, K., Three-dimensional visualization in powder diffraction, *Solid State Phenomena* **2007**, *130*, 15-20.

(18) Komarek, A. C.; Streltsov, S. V.; Isobe, M.; Möller, T.; Hoelzel, M.; Senyshyn, A.; Trots, D.; Fernández-Díaz, M. T.; Hansen, T.; Gotou, H.; Yagi, T.; Ueda, Y.; Anisimov, V. I.; Grüninger, M.; Khomskii, D. I.; Braden, M., $CaCrO_3$: An Anomalous Antiferromagnetic Metallic Oxide, *Phys. Rev. Lett.* **2008**, *101*, 167204.

(19) Sarma, D. D.; Maiti, K.; Vescovo, E.; Carbone, C.; Eberhardt, W.; Rader, O.; Gudat, W., Investigation of hole-doped insulating $La_{1-x}Sr_xCrO_3$ by soft-x-ray absorption spectroscopy, *Physical Review* **1996**, *53*, 13369.

(20) Komarek, A. C.; Möller, T.; Isobe, M.; Drees, Y.; Ulbrich, H.; Azuma, M.; Fernández-Díaz, M. T.; Senyshyn, A.; Hoelzel, M.; André, G.; Ueda, Y.; Grüninger, M.; Braden, M., Magnetic order, transport and infrared optical properties in the $ACrO_3$ system (A = Ca, Sr, and Pb), *Phys. Rev. B* **2011**, *84*, 125114.

(21) Goldschmidt, V. M., Crystal structure and chemical constitution, *Trans. Faraday Soc.* **1929**, *25*, 253-283.

(22) Shannon, R. D., Revised effective ionic radii and systematic studies of interatomic distances in halides and chalcogenides, *Acta Cryst.* **1976**, *A32*, 751-767.

(23) Shinawi, H. E.; Marco, J. F.; Berry, F. J.; Greaves, C., $LaSrCoFeO_5$, $LaSrCoFeO_5F$ and $LaSrCoFeO_{5.5}$: new La–Sr–Co–Fe perovskites, *J. Mater. Chem.* **2010**, *20*, 3253-3259.

(24) Clemens, O.; Kuhn, M.; Haberkorn, R., Synthesis and characterization of the $La_{1-x}Sr_xFeO_{3-\delta}$ system and the fluorinated phases $La_{1-x}Sr_xFeO_{3-x}F_x$, *J. Solid State Chem.* **2011**, *184*, 2870-2876.

(25) Mitra, C.; Meyer, T.; Lee, H. N.; Reboredo, F. A., Oxygen diffusion pathways in brownmillerite $SrCoO_{2.5}$: Influence of structure and chemical potential, *The Journal of chemical physics* **2014**, *141*, 084710.

(26) Tsujimoto, Y.; Yamaura, K.; Hayashi, N.; Kodama, K.; Igawa, N.; Matsushita, Y.; Katsuya, Y.; Shirako, Y.; Akaogi, M.; Takayama-Muromachi, E., Topotactic Synthesis and Crystal Structure of a Highly Fluorinated Ruddlesden–Popper-Type Iron Oxide, $Sr_3Fe_2O_{5+x}F_{2-x}$($x \approx 0.44$), *Chemistry of Materials* **2011**, *23*, 3652-3658.

(27) Blakely, C. K.; Davis, J. D.; Bruno, S. R.; Kraemer, S. K.; Zhu, M.; Ke, X.; Bi, W.; Alp, E. E.; Poltavets, V. V., Multistep synthesis of the $SrFeO_2F$ perovskite oxyfluoride via the $SrFeO_2$ infinite-layer intermediate, *Journal of Fluorine Chemistry* **2014**, *159*, 8-14.

(28) Damay, F.; Martin, C.; Hardy, V.; Maignan, A.; André, G.; Knight, K.; Giblin, S. R.; Chapon, L. C., Zigzag ladders with staggered magnetic chirality in the S=3/2 compound β-$CaCr_2O_4$, *Phys. Rev. B* **2010**, *81*, 214405.

(29) Bhobe, P. A.; Chainani, A.; Taguchi, M.; Eguchi, R.; Matsunami, M.; Ohtsuki, T.; Ishizaka, K.; Okawa, M.; Oura, M.; Senba, Y.; Ohashi, H.; Isobe, M.; Ueda, Y.; Shin, S., Electronic structure of an antiferromagnetic metal: $CaCrO_3$, *Phys. Rev. B* **2011**, *83*, 165132.

(30) Cheng, J. G.; Sui, Y.; Zhou, J. S.; Goodenough, J. B.; Su, W. H., Transition from Orbital Liquid to Jahn-Teller Insulator in Orthorhombic Perovskites $RTiO_3$, *Phys. Rev. Lett.* **2008**, *101*, 087205.

(31) Zhou, J. S.; Ren, Y.; Yan, J. Q.; Mitchell, J. F.; Goodenough, J. B., Frustrated Superexchange Interaction Versus Orbital Order in a $LaVO_3$ Crystal, *Phys. Rev. Lett.* **2008**, *100*, 046401.

Table of Contents Entry

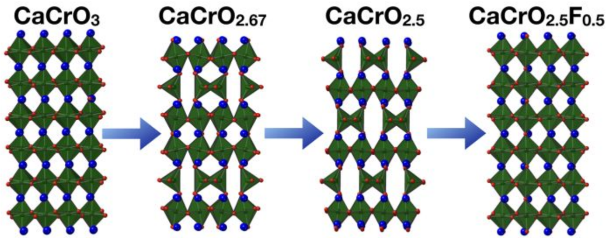

$CaCrO_3$ synthesized by high pressure methods is topochemically treated with polyvinylidene difluoride and undergoes stepwise reduction followed by fluorine incorporation.